

Spin-phonon interaction and short-range order in $\text{Mn}_3\text{Si}_2\text{Te}_6$

S. Djurdjic Mijin,¹ A. Šolajić,¹ J. Pešić,^{1,*} Y. Liu,^{2,†} C. Petrovic,² M. Bockstedte,³ A. Bonanni,⁴
Z. V. Popović,^{1,5} and N. Lazarević¹

¹*Institute of Physics Belgrade, University of Belgrade, Pregrevica 118, 11080 Belgrade, Serbia*

²*Condensed Matter Physics and Materials Science Department, Brookhaven National Laboratory, Upton, New York 11973-5000, USA*

³*Institute for Theoretical Physics, Johannes Kepler University Linz, Altenbergerstrasse 69, 4040 Linz, Austria*

⁴*Institute of Semiconductor and Solid-State Physics, Johannes Kepler University Linz, Altenbergerstrasse 69, 4040 Linz, Austria*

⁵*Serbian Academy of Sciences and Arts, Knez Mihailova 35, 11000 Belgrade, Serbia*



(Received 7 September 2022; revised 31 January 2023; accepted 3 February 2023; published 21 February 2023)

The vibrational properties of ferrimagnetic $\text{Mn}_3\text{Si}_2\text{Te}_6$ single crystals are investigated using Raman spectroscopy and density functional theory calculations. Eighteen Raman-active modes are identified, 14 of which are assigned according to the trigonal symmetry. Four additional peaks, obeying the A_{1g} selection rules, are attributed to the overtones. The unconventional temperature evolution of the A_{1g}^5 mode self-energy suggests a competition between different short-range magnetic correlations that significantly impact the spin-phonon interaction in $\text{Mn}_3\text{Si}_2\text{Te}_6$. The research provides comprehensive insight into the lattice properties, studies their temperature dependence, and shows arguments for the existence of competing short-range magnetic phases in $\text{Mn}_3\text{Si}_2\text{Te}_6$.

DOI: [10.1103/PhysRevB.107.054309](https://doi.org/10.1103/PhysRevB.107.054309)

I. INTRODUCTION

Layered magnetic van der Waals materials have lately received widespread attention due to their potential application in spintronics, magnetoelectronics, data storage, and biomedicine [1–7]. Recent experimental confirmation of a long-range magnetism persisting down to a monolayer in CrI_3 [8] further affirmed these materials as a platform for magneto-optoelectronic devices [9], and as candidates for studying low-dimensional magnetism [10].

$\text{Mn}_3\text{Si}_2\text{Te}_6$ single crystals were first synthesized in 1985 [11]. However, few studies were carried out on this compound since. It was only recently that the attention has shifted to them, mainly through comparisons with quasi-two-dimensional materials, specifically CrSiTe_3 . The vast majority of recent studies were focused on explaining the magnetism in $\text{Mn}_3\text{Si}_2\text{Te}_6$ and determining its crystal structure. It was revealed that $\text{Mn}_3\text{Si}_2\text{Te}_6$ crystallizes in a trigonal structure described by the $P\bar{3}1c$ (No. 163) space group [11,12]. According to various magnetization studies, $\text{Mn}_3\text{Si}_2\text{Te}_6$ is an insulating ferrimagnetic with Curie temperature T_c between 74 and 78 K [12–15]. First-principles calculations suggested a competition between the ferrimagnetic ground state and three additional magnetic configurations, originating from the antiferromagnetic exchange for the three nearest Mn-Mn pairs [15]. Additionally, both magnetization and diffuse neutron scattering experiments point at the existence of strong spin correlations well above T_c , which may be associated with

short-range order or to the preserved correlated excitations in the paramagnetic region [12,15].

Here, we present an experimental and theoretical Raman scattering study of $\text{Mn}_3\text{Si}_2\text{Te}_6$ single crystals, with the focus on phonon properties in the temperature range from 80 to 320 K. Out of 18 observed modes, 14 ($5A_{1g} + 9E_g$) are identified and assigned in agreement with the $P\bar{3}1c$ space group. Phonon energies are in a good agreement with the theoretical predictions. Two most prominent Raman modes, A_{1g}^4 and A_{1g}^5 , are used to study the temperature evolution of phonon properties, and reveal three subsequent phase transitions at $T_1 = 142.5$ K, $T_2 = 190$ K, and $T_3 = 285$ K. Furthermore, the A_{1g}^5 mode exhibits strong asymmetry, most likely originating from enhanced spin-phonon coupling. Interestingly, the A_{1g}^5 phonon line is symmetric in the temperature range T_1 – T_2 , while becoming more asymmetric above T_3 , potentially indicating that the strength of spin-phonon interaction changes with temperature. We speculate that the observed phenomenon, shown in the A_{1g}^5 phonon, originates from the shift in dominance between competing magnetic states, that are found to be very close in energy [15].

II. EXPERIMENTAL AND COMPUTATIONAL DETAILS

The $\text{Mn}_3\text{Si}_2\text{Te}_6$ single-crystal samples used in this study are prepared according to the procedure described in Ref. [12]. The Raman spectra have been obtained with a Tri Vista 557 spectrometer (Teledyne Princeton Instruments, Trenton, NJ, USA) with a 1800/1800/2400 grooves/mm diffraction grating combination in a backscattering configuration. The 514-nm line of a Coherent Ar^+/Kr^+ ion laser (Coherent, Santa Clara, CA, USA) is utilized as the excitation source. The direction of the incident (scattered) light coincides with

*Corresponding author: jelena.pesic@ipb.ac.rs

†Present address: Los Alamos National Laboratory, Los Alamos, New Mexico 87545, USA.

TABLE I. Wyckoff positions of atoms and their contributions to the Γ -point phonons together with the corresponding Raman tensors for the $P\bar{3}1c$ space group of $\text{Mn}_3\text{Si}_2\text{Te}_6$.

Space group: $P\bar{3}1c$	
Atoms	Irreducible representations
Mn (2 <i>c</i>)	$A_{2g} + A_{2u} + E_g + E_u$
Mn (4 <i>f</i>)	$A_{1g} + A_{1u} + A_{2g} + A_{2u} + 2E_g + 2E_u$
Si (4 <i>e</i>)	$A_{1g} + A_{1u} + A_{2g} + A_{2u} + 2E_g + 2E_u$
Te (12 <i>i</i>)	$3A_{1g} + 3A_{1u} + 3A_{2g} + 3A_{2u}$ $+ 6E_g + 6E_u$
Raman tensors	
	$A_{1g} = \begin{pmatrix} a & & \\ & a & \\ & & b \end{pmatrix}$
${}^1E_g = \begin{pmatrix} c & & \\ & -c & d \\ & & d \end{pmatrix}$	${}^2E_g = \begin{pmatrix} & & -c & -d \\ & & -c & -d \\ & & & & \\ & & & & \end{pmatrix}$

the crystallographic c axis. Laser-beam focusing is achieved through a microscope objective with $50\times$ magnification. The temperature-dependent Raman scattering measurements have been performed under high vacuum (10^{-6} mbar), with the sample being placed inside of a KONTI CryoVac continuous helium flow cryostat (CryoVac GmbH & Co. KG, Troisdorf, Germany) with a 0.5-mm-thick window. The samples are cleaved in air before being placed into the cryostat. The obtained Raman spectra are corrected by a Bose factor. The spectrometer resolution is comparable to a Gaussian width of 1 cm^{-1} .

The calculations are based on the density functional theory (DFT) formalism as implemented in the Vienna *ab initio* simulation package (VASP) [16–19], with the plane-wave basis truncated at a kinetic energy of 520 eV, using the Perdew-Burke-Ernzerhof (PBE) exchange-correlation functional [20] and projector augmented-wave (PAW) method [19,21]. The Monkhorst and Pack scheme of k -point sampling is employed to integrate over the first Brillouin zone with $12 \times 12 \times 10$ at the Γ -centered grid. The convergence criteria for energy and force have been set to 10^{-6} eV and 0.001 eV \AA^{-1} , respectively. The DFT-D2 method of Grimme is employed for van der Waals (vdW) corrections [22]. The vibrational modes are calculated using density functional perturbation theory implemented in VASP and PHONOPY [23]. Previous DFT results found the energy of the ferrimagnetic state to be well above an eV per Mn below that of the nonmagnetic state [15], thus this configuration is considered in this study.

III. RESULTS AND DISCUSSION

A. Polarization measurements

$\text{Mn}_3\text{Si}_2\text{Te}_6$ crystallizes in a trigonal $P\bar{3}1c$ crystal structure [11,12]. The Wyckoff positions of the atoms and their contributions to the Γ -point phonons, together with the corresponding Raman tensors, are listed in Table I. In total, there are 16 Raman-active modes ($5A_{1g} + 11E_g$) and 17 infrared-active modes ($6A_{2u} + 11E_u$). According to the Raman tensors presented in Table I, in our scattering configuration and with

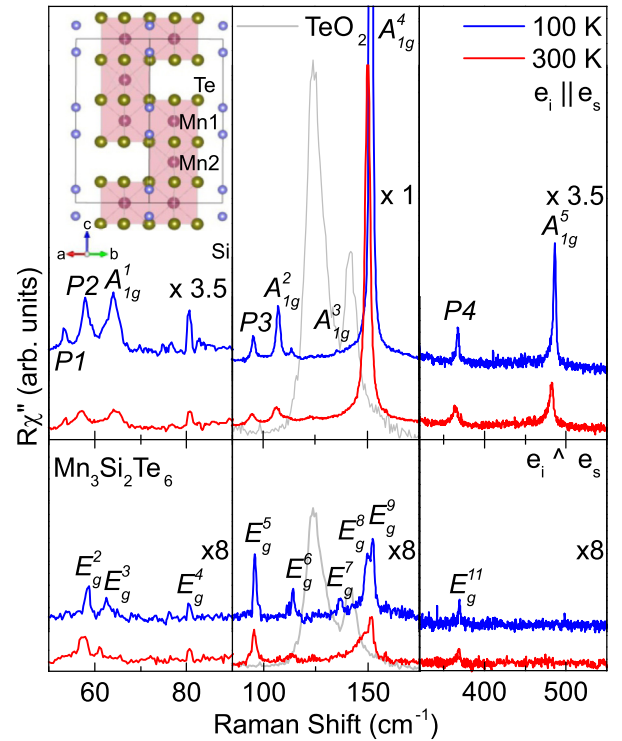


FIG. 1. Raman spectra of $\text{Mn}_3\text{Si}_2\text{Te}_6$ single crystal measured in two scattering geometries at $T = 100\text{ K}$ (blue solid line) and $T = 300\text{ K}$ (red solid lines) with incident light being directed along [100]. Peaks observed in both geometries are identified as E_g modes, whereas peaks observed only for the parallel polarization configuration are assigned as A_{1g} modes. Gray line: TeO_2 spectrum at 300 K, scaled for clarity. The crystal structure of $\text{Mn}_3\text{Si}_2\text{Te}_6$ viewed laterally along the c axis is presented in the inset.

Raman scattering events within the crystallographic ab plane, E_g symmetry modes can be observed in the Raman spectra measured in both parallel and crossed polarization configurations, whereas A_{1g} modes arise only for those in parallel polarization configuration.

As depicted in Fig. 1, nine phonon lines are observed in a parallel polarization configuration only, and identified as A_{1g} symmetry modes. According to the symmetry analysis only five A_{1g} symmetry modes are expected, resulting in four excess modes at 53.3 , 57.9 , 95.3 , and 366.7 cm^{-1} . These modes may arise from infrared/silent phonons activated by disorder and from the relaxation of the symmetry selection rules [24–27]. However, it is more likely they are overtones. Overtones, which are always observable in A symmetries, but can also be observed in other symmetries, can become observable in Raman spectra due to disorder and/or enhanced coupling of the phonons to other excitations such as in the case of spin-phonon coupling [28].

Aside from the discussed A_{1g} symmetry modes, our spectra host nine modes which obey the E_g selection rules. Therefore, nine out of the expected 11 E_g modes have been singled out and identified. The absence of two E_g modes might be attributed to their low intensity and/or the finite resolution of the spectrometer.

Calculated and experimental phonon energies are collected in Table II, and are found to be in good agreement with each

TABLE II. Phonon symmetries and phonon frequencies of $\text{Mn}_3\text{Si}_2\text{Te}_6$ phonons. The experimental values are determined at 100 K. All calculations have been performed at zero 0 K. The experimental uncertainty is 0.3 cm^{-1} .

Space group $P\bar{3}1c$			
n_0	Symm.	Expt. (cm^{-1})	Calc. (cm^{-1})
1	E_g^1		53.1
2	$P1$	53.3	
3	$P2$	57.9	
4	E_g^2	58.7	58.5
5	E_g^3	62.6	61.8
6	A_{1g}^1	64.2	62.3
7	E_g^4	80.4	82.7
8	$P3$	95.3	
9	E_g^5	95.9	90.3
10	A_{1g}^2	107.3	104.3
11	E_g^6	114.0	106.5
12	A_{1g}^3	135.4	134.2
13	E_g^7	136.6	136.1
14	E_g^8	149.8	143.4
15	A_{1g}^4	151.8	147.3
16	E_g^9	152.6	146.6
17	E_g^{10}		352.7
18	$P4$	366.7	
19	E_g^{11}	368.7	354.5
20	A_{1g}^5	486.7	475.8

other, with the discrepancy being below 8% for all observed modes.

Our data significantly differ from those presented in Ref. [14] where two Raman-active modes were reported, one at 118.4 cm^{-1} and the other at 136.9 cm^{-1} , assigned as E_g and A_{1g} , respectively. The E_g and A_{1g} modes in our spectra closest (in terms of energy) to those reported in Ref. [14] are the peaks at ~ 114.3 and 135.4 cm^{-1} (Table II). Although the discrepancy in phonon energy is not significant, the observed phonon linewidths strongly deviate from those presented in Ref. [14]. A possible explanation for the discrepancy is the presence of TeO_2 in samples presented in Ref. [14], as the peaks reported there match rather well with the Raman response of TeO_2 (Fig. 1). In order to avoid potential contamination in our study, measurements have been repeated on multiple crystals, and no oxide traces have been identified in the spectra.

B. Temperature dependence

Some of the modes represented in Fig. 1 exhibit an asymmetric line shape. Although the appearance of a mode asymmetry can be attributed to the presence of defects [29], this would have a significant impact also on the linewidths of other modes in the spectrum, which is not the case here. The asymmetry may arise from coupling between the phonon and other elementary excitations [30–32]. The line shape originating from such a coupling is given by the Fano

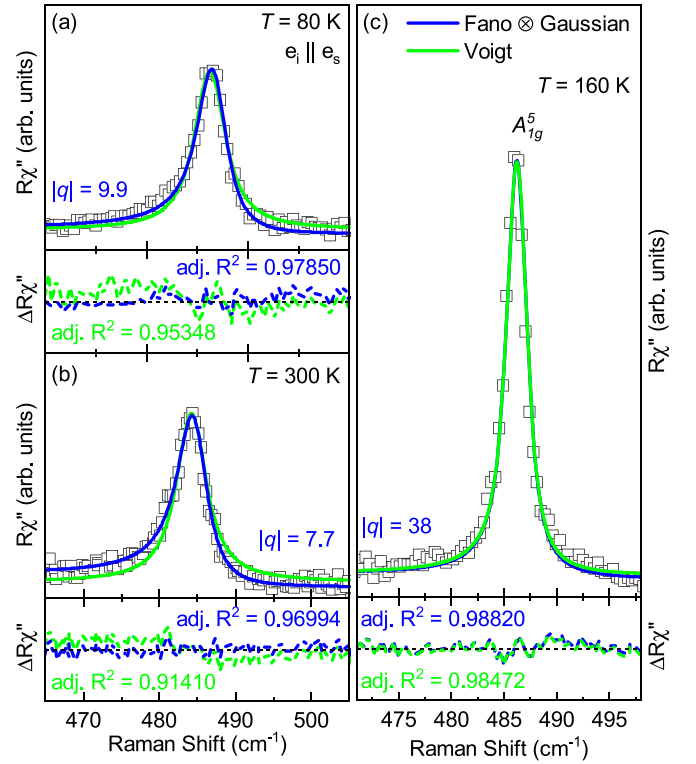


FIG. 2. Raman response as a function of the Raman shift. Quantitative analysis of the A_{1g}^5 mode at temperatures as indicated. (a) and (b) The blue solid lines represent the line shape obtained as a convolution of Fano profiles and Gaussian, whereas the green solid lines represent Voigt profiles. (c) Comparison between asymmetric (deep blue) and symmetric (light blue) line shapes obtained as a Fano-Gaussian convolution and a Voigt profile. Experimental data are represented by open squares.

profile [33–36]

$$I(\omega) = I_0 \frac{(q + \epsilon)^2}{1 + \epsilon^2},$$

where $\epsilon(\omega) = 2(\omega - \omega_0)/\Gamma$. Here, ω_0 is the phonon frequency in the absence of interaction, Γ is the full width at half maximum (FWHM), I_0 is the amplitude, and q is the Fano parameter. The Fano parameter and FWHM depend on the interaction strength between the phonon and the elementary excitation, and therefore can be used as its indicator. To include the finite spectral resolution of the experimental setup, the Fano profile is convoluted with a Gaussian function as demonstrated in Ref. [28].

The high-intensity peak at 486.7 cm^{-1} , identified as the A_{1g}^5 symmetry mode, does not overlap with any other mode. The quantitative analysis of this peak is performed using both the symmetric Voigt profile and the Fano-Gaussian convolution mentioned above. The comparison between the two models and the experimental data at 80 and 300 K are presented in Figs. 2(a) and 2(b), respectively. The asymmetric line shapes provide a satisfactory description of the measured phonon line shape, suggesting the presence of an additional scattering mechanism in $\text{Mn}_3\text{Si}_2\text{Te}_6$.

The spectral region of the A_{1g}^5 Raman-active mode in the temperature range of interest is presented in Fig. 3(a). The

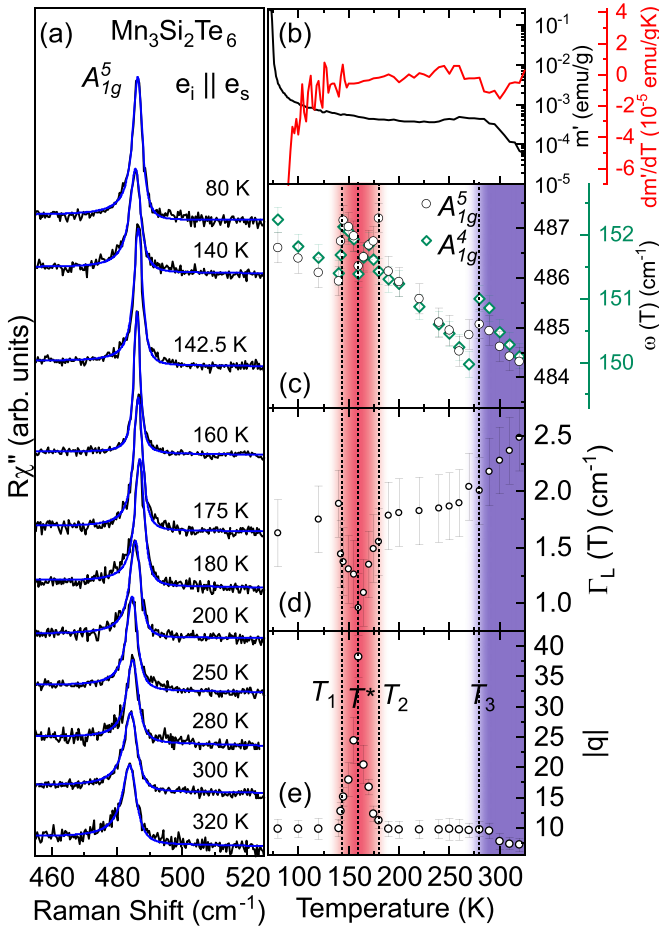


FIG. 3. (a) The spectral region of the A_{1g}^5 Raman-active mode of $\text{Mn}_3\text{Si}_2\text{Te}_6$ at indicated temperatures measured in the parallel polarization configuration. Green solid lines represent line shapes obtained as a convolution of the Fano line shape and Gaussian, calculated to fit the experimental data. (b) Temperature dependence of ac susceptibility real part $m'(T)$ and its temperature derivative plotted as a function of temperature with $\mathbf{H} \parallel \mathbf{ab}$. Temperature dependence of (c) the energy of the A_{1g}^4 and A_{1g}^5 as well as (d) the linewidth, and (e) the Fano parameter $|q|$ of the A_{1g}^5 mode.

blue solid lines represent fits to the experimental data obtained using the Fano-Gaussian line shape. The temperature dependence of the phonon energy, linewidth, and the Fano parameter $|q|$ of the A_{1g}^5 mode are depicted in Figs. 3(c)–3(e), respectively. By increasing the temperature above 80 K, the A_{1g}^5 mode broadens and softens up to $T_1 = 142.5$ K, where it abruptly narrows and shifts to higher energies followed by further softening and narrowing up to $T^* = 160$ K. Additional heating leads to a broadening and hardening before the drop in phonon energy at $\sim T_2 = 190$ K. In the region T_2 the mode softens and broadens with an additional jump in phonon energy at $T_3 = 285$ K. A similar trend is also observed for the A_{1g}^4 mode, as evidenced in Fig. 3(b).

This intriguing temperature dependence is also manifested in the asymmetry, i.e., the Fano parameter $|q|$ [Fig. 3(d)] of the A_{1g}^5 peak. At the lowest experimental temperature, 80 K, the A_{1g}^5 mode exhibits strong asymmetry with a Fano parameter $|q| = 9.9$. Upon heating the sample to $\sim T_1$ a Fano parameter

remains nearly constant before the significant increase in the temperature range between T_1 and T^* resulting in a symmetric line shape [$|q| = 38$, Fig. 3(c)]. A further temperature increase leads to a strong decrease of $|q|$ up to T_2 , where the asymmetry is restored ($|q| = 9.9$), remaining almost constant up to T_3 . At higher temperatures, the line shape becomes more asymmetric, reaching $|q| \sim 8$ at the highest experimentally accessible temperature $T = 320$ K.

While the ferrimagnetic order in $\text{Mn}_3\text{Si}_2\text{Te}_6$ is established only at $T_c = 78$ K [12,14], the asymmetry of the mode can be observed at all experimental temperatures. Based on the research done on $\text{Mn}_3\text{Si}_2\text{Te}_6$ and related materials, the most probable scenario is the one in which the observed asymmetry can be traced to an enhanced spin-phonon interaction related to short-range correlations, that can survive up to temperatures well above T_c [24,37–39]. We may speculate, according to the results presented in Ref. [15], that these short-range correlations are likely in terms of the antiferromagnetic exchange interaction between the three nearest Mn-Mn pairs (as depicted in Fig. 1) in the paramagnetic background. However, this alone cannot explain sudden changes in the properties of the A_{1g}^5 phonon mode. Rather, the existence of competing short-range magnetic phases may be responsible for the observed behavior of the phonon modes. The first phonon mode anomaly at $T_3 = 285$ K corresponds to the anomaly in $m'(T)_{ab}$ [Fig. 3(b)] and can be seen as the outlet of additional short-range order in the paramagnetic domains [40] and possibly change of their nature of previously established ones. The onset in temperature with the magnetization anomaly near 330 K [14,41] is likely the consequence of local disorder. At T_2 , $\text{Mn}_3\text{Si}_2\text{Te}_6$ becomes locally magnetically frustrated, resulting in the change in magnetostriction and a rapid decrease of the spin-phonon interaction that is manifested in the strong evolution of the phonon self-energy (Fig. 3). At this temperature both the magnetoresistance and nonlinearity of Hall resistance become observable [41]. In this scenario, by further lowering the temperature, at T_1 a new short-range magnetic order and the strong spin-phonon interaction are established. The new magnetic order is most likely antiferromagnetic [15]. In order to fully understand the complex evolution of the short-range magnetic correlation in $\text{Mn}_3\text{Si}_2\text{Te}_6$ that is manifested through the anomalous temperature development of the A_{1g}^5 mode, further investigations are required.

IV. CONCLUSION

The lattice dynamic in single-crystalline $\text{Mn}_3\text{Si}_2\text{Te}_6$ using Raman spectroscopy in analyzed. Five A_{1g} modes and nine E_g modes are observed and assigned according to the $P\bar{3}1c$ symmetry group. Four additional peaks to the ones assigned to the $P\bar{3}1c$ symmetry group, obeying A_{1g} selection rules, are attributed to overtones. There is a pronounced asymmetry of the A_{1g}^5 phonon mode at 100 and 300 K. The unconventional temperature evolution of the A_{1g}^5 Raman mode reveals three successive, possibly magnetic, phase transitions that may significantly impact the strength of the spin-phonon interaction in $\text{Mn}_3\text{Si}_2\text{Te}_6$. These are likely caused by the competition between the various magnetic states, close in energy. This paper provides comprehensive insight into the lattice properties, their temperature dependence, and shows arguments

for the existence of competing short-range magnetic phases in $\text{Mn}_3\text{Si}_2\text{Te}_6$.

ACKNOWLEDGMENTS

The authors acknowledge funding provided by the Institute of Physics Belgrade, through a grant from the Ministry of Science, Technological Development and Innovations of the Republic of Serbia, the Serbian Academy of Sciences and Arts - Project No. F-134, the Science Fund of the Republic of

Serbia, PROMIS, 6062656, StrainedFeSC, Austrian Science Fund (FWF) through Project No. P31423, and the support of Austrian Academy of Sciences' Joint Excellence in Science and Humanities (JESH) Program (J.P.). DFT calculations were performed using computational resources at Johannes Kepler University (Linz, Austria). Materials synthesis was supported by the U.S. DOE-BES, Division of Materials Science and Engineering, under Contract No. DE-SC0012704 (BNL). The authors would like to thank Dr. Rudi Hackl for useful discussions that contributed to the finalized version of the manuscript.

- [1] Z. Guguchia, Unconventional magnetism in layered transition metal dichalcogenides, *Condensed Matter* **5**, 42 (2020).
- [2] Q. H. Wang, K. Kalantar-Zadeh, A. Kis, J. N. Coleman, and M. S. Strano, Electronics and optoelectronics of two-dimensional transition metal dichalcogenides, *Nat. Nanotechnol.* **7**, 699 (2012).
- [3] W. Han, R. K. Kawakami, M. Gmitra, and J. Fabian, Graphene spintronics, *Nat. Nanotechnol.* **9**, 794 (2014).
- [4] W. Zhang, R. Mazzarello, M. Wuttig, and E. Ma, Designing crystallization in phase-change materials for universal memory and neuro-inspired computing, *Nat. Rev. Mater.* **4**, 150 (2019).
- [5] C. Zhu, G. Yang, H. Li, D. Du, and Y. Lin, Electrochemical sensors and biosensors based on nanomaterials and nanostructures, *Anal. Chem.* **87**, 230 (2015).
- [6] X. J. Zhou, Magnetism in medicine: A handbook, second completely revised and enlarged edition, *Med. Phys.* **34**, 4978 (2007).
- [7] Q. H. Wang, A. Bedoya-Pinto, M. Blei, A. H. Dismukes, A. Hamo, S. Jenkins, M. Koperski, Y. Liu, Q.-C. Sun, E. J. Telford, H. H. Kim, M. Augustin, U. Vool, J.-X. Yin, L. H. Li, A. Falin, C. R. Dean, F. Casanova, R. F. L. Evans, M. Chshiev *et al.*, The magnetic genome of two-dimensional van der Waals materials, *ACS Nano* **16**, 6960 (2022).
- [8] B. Huang, G. Clark, E. Navarro-Moratalla, D. R. Klein, R. Cheng, K. L. Seyler, D. Zhong, E. Schmidgall, M. A. McGuire, D. Cobden, W. Yao, D. Xiao, P. Jarillo-Herrero, and X. Xu, Layer-dependent ferromagnetism in a van der Waals crystal down to the monolayer limit, *Nature (London)* **546**, 270 (2017).
- [9] S. Jiang, L. Li, Z. Wang, K. F. Mak, and J. Shan, Controlling magnetism in 2D CrI_3 by electrostatic doping, *Nat. Nanotechnol.* **13**, 549 (2018).
- [10] N. Sethulakshmi, A. Mishra, P. Ajayan, Y. Kawazoe, A. K. Roy, A. K. Singh, and C. S. Tiwary, Magnetism in two-dimensional materials beyond graphene, *Mater. Today* **27**, 107 (2019).
- [11] H. Vincent, D. Leroux, and D. Bijaoui, Crystal structure of $\text{Mn}_3\text{Si}_2\text{Te}_6$, *J. Solid State Chem.* **63**, 349 (1986).
- [12] Y. Liu and C. Petrovic, Critical behavior and magnetocaloric effect in $\text{Mn}_3\text{Si}_2\text{Te}_6$, *Phys. Rev. B* **98**, 064423 (2018).
- [13] R. Rimet, C. Schlenker, and H. Vincent, A new semiconducting ferrimagnet: A silicon manganese telluride, *J. Magn. Magn. Mater.* **25**, 7 (1981).
- [14] L. M. Martinez, H. Iturriaga, R. Olmos, L. Shao, Y. Liu, T. T. Mai, C. Petrovic, A. R. Hight Walker, and S. R. Singamaneni, Enhanced magnetization in proton irradiated $\text{Mn}_3\text{Si}_2\text{Te}_6$ van der Waals crystals, *Appl. Phys. Lett.* **116**, 172404 (2020).
- [15] A. F. May, Y. Liu, S. Calder, D. S. Parker, T. Pandey, E. Cakmak, H. Cao, J. Yan, and M. A. McGuire, Magnetic order and interactions in ferrimagnetic $\text{Mn}_3\text{Si}_2\text{Te}_6$, *Phys. Rev. B* **95**, 174440 (2017).
- [16] G. Kresse and J. Hafner, *Ab initio* molecular dynamics for liquid metals, *Phys. Rev. B* **47**, 558 (1993).
- [17] G. Kresse and J. Furthmüller, Efficiency of ab-initio total energy calculations for metals and semiconductors using a plane-wave basis set, *Comput. Mater. Sci.* **6**, 15 (1996).
- [18] G. Kresse and J. Furthmüller, Efficient iterative schemes for *ab initio* total-energy calculations using a plane-wave basis set, *Phys. Rev. B* **54**, 11169 (1996).
- [19] G. Kresse and D. Joubert, From ultrasoft pseudopotentials to the projector augmented-wave method, *Phys. Rev. B* **59**, 1758 (1999).
- [20] J. P. Perdew, K. Burke, and M. Ernzerhof, Generalized Gradient Approximation Made Simple, *Phys. Rev. Lett.* **77**, 3865 (1996).
- [21] P. E. Blöchl, Projector augmented-wave method, *Phys. Rev. B* **50**, 17953 (1994).
- [22] S. Grimme, Semiempirical GGA-type density functional constructed with a long-range dispersion correction, *J. Comput. Chem.* **27**, 1787 (2006).
- [23] A. Togo and I. Tanaka, First principles phonon calculations in materials science, *Scr. Mater.* **108**, 1 (2015).
- [24] F. Jin, N. Lazarević, C. Liu, J. Ji, Y. Wang, S. He, H. Lei, C. Petrovic, R. Yu, Z. V. Popović, and Q. Zhang, Phonon anomalies and magnetic excitations in $\text{BaFe}_2\text{Se}_2\text{O}$, *Phys. Rev. B* **99**, 144419 (2019).
- [25] M. Moskovits and D. Dilella, Surface-enhanced Raman spectroscopy of benzene and benzene- d_6 adsorbed on silver, *J. Chem. Phys.* **73**, 6068 (1980).
- [26] A. Dubroka, J. Humlíček, M. V. Abrashev, Z. V. Popović, F. Sapiña, and A. Cantarero, Raman and infrared studies of $\text{La}_{1-y}\text{Sr}_y\text{Mn}_{1-x}\text{M}_x\text{O}_3$ ($M = \text{Cr, Co, Cu, Zn, Sc, or Ga}$): Oxygen disorder and local vibrational modes, *Phys. Rev. B* **73**, 224401 (2006).
- [27] A. G. Souza Filho, J. L. B. Faria, I. Guedes, J. M. Sasaki, P. T. C. Freire, V. N. Freire, J. Mendes Filho, M. M. Xavier, F. A. O. Cabral, J. H. de Araújo, and J. A. P. da Costa, Evidence of magnetic polaronic states in $\text{La}_{0.70}\text{Sr}_{0.30}\text{Mn}_{1-x}\text{Fe}_x\text{O}_3$ manganites, *Phys. Rev. B* **67**, 052405 (2003).
- [28] A. Baum, A. Milosavljević, N. Lazarević, M. M. Radonjić, B. Nikolić, M. Mitschek, Z. I. Maranloo, M. Šćepanović, M. Grujić-Brojčin, N. Stojilović, M. Opel, A. Wang, C. Petrovic,

- Z. V. Popović, and R. Hackl, Phonon anomalies in FeS, *Phys. Rev. B* **97**, 054306 (2018).
- [29] N. Lazarević, M. Radonjić, M. Šćepanović, H. Lei, D. Tanasković, C. Petrovic, and Z. V. Popović, Lattice dynamics of KNi_2Se_2 , *Phys. Rev. B* **87**, 144305 (2013).
- [30] M. Balkanski, K. P. Jain, R. Beserman, and M. Jouanne, Theory of interference distortion of Raman scattering line shapes in semiconductors, *Phys. Rev. B* **12**, 4328 (1975).
- [31] D. Olego and M. Cardona, Self-energy effects of the optical phonons of heavily doped p -GaAs and p -Ge, *Phys. Rev. B* **23**, 6592 (1981).
- [32] E. H. Hasdeo, A. R. T. Nugraha, M. S. Dresselhaus, and R. Saito, Breit-Wigner-Fano line shapes in Raman spectra of graphene, *Phys. Rev. B* **90**, 245140 (2014).
- [33] U. Fano, Effects of configuration interaction on intensities and phase shifts, *Phys. Rev.* **124**, 1866 (1961).
- [34] P. H. M. van Loosdrecht, J. P. Boucher, G. Martinez, G. Dhalenne, and A. Revcolevschi, Inelastic Light Scattering from Magnetic Fluctuations in CuGeO_3 , *Phys. Rev. Lett.* **76**, 311 (1996).
- [35] M. Braden, B. Hennion, W. Reichardt, G. Dhalenne, and A. Revcolevschi, Spin-Phonon Coupling in CuGeO_3 , *Phys. Rev. Lett.* **80**, 3634 (1998).
- [36] J. W. Ager, W. Walukiewicz, M. McCluskey, M. A. Plano, and M. I. Landstrass, Fano interference of the Raman phonon in heavily boron-doped diamond films grown by chemical vapor deposition, *Appl. Phys. Lett.* **66**, 616 (1995).
- [37] S. Djurdjić Mijin, A. M. M. Abeykoon, A. Šolajić, A. Milosavljević, J. Pešić, Y. Liu, C. Petrovic, Z. V. Popović, and N. Lazarević, Short-range order in VI_3 , *Inorg. Chem.* **59**, 16265 (2020).
- [38] L. J. Sandilands, Y. Tian, K. W. Plumb, Y.-J. Kim, and K. S. Burch, Scattering Continuum and Possible Fractionalized Excitations in α - RuCl_3 , *Phys. Rev. Lett.* **114**, 147201 (2015).
- [39] A. Milosavljević, A. Šolajić, J. Pešić, Y. Liu, C. Petrovic, N. Lazarević, and Z. V. Popović, Evidence of spin-phonon coupling in CrSiTe_3 , *Phys. Rev. B* **98**, 104306 (2018).
- [40] Y. Liu, Z. Hu, M. Abeykoon, E. Stavitski, K. Attenkofer, E. D. Bauer, and C. Petrovic, Polaronic transport and thermoelectricity in $\text{Mn}_3\text{Si}_2\text{Te}_6$ single crystals, *Phys. Rev. B* **103**, 245122 (2021).
- [41] Y. Ni, H. Zhao, Y. Zhang, B. Hu, I. Kimchi, and G. Cao, Colossal magnetoresistance via avoiding fully polarized magnetization in the ferrimagnetic insulator $\text{Mn}_3\text{Si}_2\text{Te}_6$, *Phys. Rev. B* **103**, L161105 (2021).